Cornell University

Sibley School of Mechanical and Aerospace Engineering

Liquid Drop Falling Through a Quiescent Gas at Terminal Velocity

A Project Report
Presented to the Engineering Division of the Graduate School
of Cornell University
in Partial Fulfilment of the Requirements for the Degree of
Master of Engineering (Mechanical)

By
Neola Putnam
Project Advisor: Olivier Desjardins
Degree Date: May 2014

1 Introduction

A liquid droplet falling at terminal velocity through a quiescent gas experiences a balance of gravity and drag forces. Though this is a common physical multiphase phenomenon (e.g., raindrops), the use of numerical methods to model droplet behavior generally have been limited to axisymmetric models with little droplet deformation [1]. As the inertial effects lead to drop deformation, many computational methods have difficulty in tracking the droplet interface without introducing significant amounts of computational error, especially in the presence of the large density ratio at the gas-liquid interface. Analytical closed-form solutions are also very limited in predicting droplet behavior: they exist for inviscid or highly viscous flow assumptions, with the additional assumption that the droplet remains nearly spherical [1].

A relevant computational model of liquid droplets must accurately track the interface between the two immiscible fluids. The gas and liquid are characterized by a high density ratio which, combined with the velocity difference between the two phases (drop internal circulation is slow compared to the drop's velocity through the air), can lead to significant numerical errors in tracking momentum. Specifically, models fail when they incorrectly locate the interface and predict a region of high density liquid phase traveling at high velocity.

The relevant dimensionless numbers characterizing this flow are as follows. The density ratio $\rho \equiv \rho_l/\rho_g$ and viscosity ratio $\mu \equiv \mu_l/\mu_g$ characterize the ratio of liquid to gas phase properties. For this project, it was desired to study values typical for water and air: a density ratio of 1000 and 100 for the viscosity ratio. Two other significant dimensionless numbers for such an analysis are Reynolds number and Weber number.

$$Re = \frac{\rho_g U D}{\mu_g} \tag{1}$$

$$We = \frac{\rho_g U^2 D}{\sigma} \tag{2}$$

where U is the drop velocity, D the characteristic drop diameter, and σ the surface tension coefficient between water and air. Reynolds number characterizes inertial to viscous forces and Weber number characterizes inertia to surface tension forces. By characterizing the flow with these dimensionless numbers, the differences observed in drop behavior can be correlated to how the multiphase flow depends on physical parameters.

Beard [2] introduced a relevant multiphase regime classification for falling drops:

- Small cloud droplets: $1\mu\text{m} \leq D \leq 20\mu\text{m}$ (steady wake, $10^{-6} \leq \text{Re} \leq 0.01$).
- Large cloud droplets to small raindrops: $20\mu\text{m} \leq D \leq 1\text{mm}$ (steady wake, $0.01 \leq \text{Re} \leq 300$)
- Small to large raindrops: $1\text{ mm} \leq D \leq 7\text{ mm}$ (unsteady wake, $300 \leq \text{Re} \leq 4000$).

The overarching goal of this project was to apply the piecewise linear interface calculation (PLIC) volume-of-fluid (VOF) method that incorporates a three-dimensional, un-split, discretely conservative, and bounded computation scheme as developed by Owkes and Desjardins [3] to the phenomenon of a liquid droplet falling through gas. Although many experiments and some theoretical analysis has been conducted to characterize drop terminal velocity and shape, few numerical simulations have been developed that effectively predict the liquid/gas interface at intermediate to high Reynolds numbers characterized by Beard's [2] second and third regime categories. The focus of this project was to verify the code's ability to predict the location of the interface and to accurately predict the terminal velocity of a falling droplet.

The classical theoretical method to predict the terminal velocity of a falling liquid drop for very small Reynolds numbers is given in the Hadamard-Rybczynski equation [1]. Two of the most definitive experimental measurements of drop terminal velocities for a range of drop sizes have been those of Gunn and Kinzer [4] and Beard and Pruppacher [5]. In a later work, Beard [2] collected several primary experimental sources and summarized the data in empirical formulas for terminal velocity. For larger ellipsoidal drops that depart from spherical, Clift, Grace, and Weber [1] recommend empirical equations be used to calculate a "correlation Reynolds number" that can then be compared directly to Gunn and Kinzer or Beard and Pruppachers experimental data.

Droplet deformation is characterized by a flattening of the drop at the front (lower) surface as a result of the increased hydrodynamic pressure. Deformation increases as inertia dominates over surface tension. One theoretical treatment of drop deformation, McDonald [6], used a distribution of aerodynamics pressure deduced from photographs of droplets traveling at terminal velocity to determine drop deformation. Taylor and Acrivos [7] outlined a method for calculating the theoretical deformation and drag of a falling drop, but restricted their analysis to low Reynolds numbers (and hence only very small deformations). Pruppacher and Pitter [8] improved an earlier method of balancing normal stresses at the interface by incorporating better experimental pressure distributions. One particularly relevant numerical prediction, Feng [9], used a Galerkin finite-element method to solve steady axisymmetric Navier-Stokes equations and elliptic mesh-generation equations for deformable drops characterized by a density ratio of ~ 1000 and a viscosity ratio of ~ 100. However, because of the axisymmetric assumption, Feng's results are limited to low to intermediate Reynolds numbers.

2 Mathematical Formulation

This section introduces the equations that describe the carrier and droplet fluid flows. Both are described by the Navier-Stokes equations for a low Mach number, variable density flow. Continuity for the carrier phase is given by

$$\frac{\partial \rho_c}{\partial t} + \nabla \cdot (\rho_c \mathbf{u}_c) = 0 \tag{3}$$

where ρ_c and $\mathbf{u}_c$ are the point wise carrier fluid density and velocity. The droplet is described similarly (changing the subscript c to d). Conservation of momentum for the carrier phase is expressed as follows (similarly for the droplet as done with continuity):

$$\frac{\partial}{\partial t}(\rho_c \mathbf{u}_c) + \nabla \cdot (\rho_c \mathbf{u}_c \otimes \mathbf{u}_c) = \nabla \cdot \boldsymbol{\tau} + \rho_c \mathbf{g} \tag{4}$$

where $\mathbf{g}$ is the acceleration due to gravity, and $\boldsymbol{\tau}$ is the point wise value of the fluid stress tensor given by

$$\boldsymbol{\tau} = -p\mathbf{I} + \mu \left[\nabla \mathbf{u}_c + \nabla \mathbf{u}_c^T - \frac{2}{3}(\nabla \cdot \mathbf{u}_c)\mathbf{I} \right] \tag{5}$$

The hydrodynamic pressure is given by p, dynamic viscosity coefficient by μ, and the identity tensor by $\mathbf{I}$.

The no-slip condition at the phase interface is given by a continuous zero velocity between the phases,

$$[\mathbf{u}]_\Gamma = 0 \tag{7}$$

discontinuous density and viscosity at the interface between the two phases,

$$[\rho]_\Gamma = \rho_l - \rho_g \tag{8}$$

$$[\mu]_\Gamma = \mu_l - \mu_g \tag{9}$$

and finally, a pressure jump at the interface due to surface tension and the velocity gradient.

$$[p]_\Gamma = \sigma\kappa + 2[\mu]_\Gamma \mathbf{n}^T \cdot \nabla\mathbf{u} \cdot \mathbf{n} \tag{10}$$

3 Solution Methodology

Several computational models have been developed to simulate multiphase flow. Volume-of-fluid (VOF) methods track the interface between the two phases by computing the liquid volume fraction and surface normal for each cell. This method, first developed by DeBar [10], Hichols and Hirt [11], and Noh and Woodward [12], is attractive because it can provide discrete mass conservation. The level-set method, introduced initially by Osher and Sethian [13], models the phase interface through the use of an iso-level of a smooth function. Unlike the VOF method, it cannot ensure mass conservation. In his use of the Galerkin finite element method of a falling drop, Feng [9] used a boundary-fitted mesh. The mesh interface was recomputed at each time step, and the flow was treated as two independent single phase flows coupled at the interface. Hybrid methods have also been used to combine the positive characteristics of some methods.

Owkes and Desjardins' [3] VOF model was used for this investigation. The computational domain is a reference frame that "falls" with the droplet: a 2D schematic is shown in Figure 1. A moving reference frame is employed because without it, the computational domain would be very large and numerically expensive. For example, a 0.5 mm water droplet, falling through air at standard conditions, would take a distance approximately 1000 times the drop diameter to reach terminal velocity.

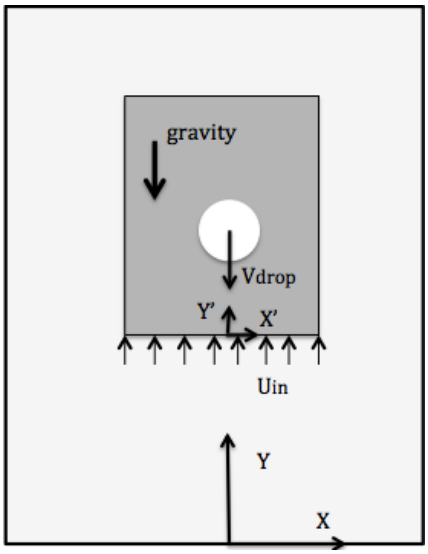

Figure 1: Schematic diagram of the moving reference frame associated with the falling droplet.

To simulate the moving reference frame, an inflow carrier phase velocity condition is applied at the boundary in the opposite direction in which a gravity force is applied. The flow field is initialized with the droplet at rest and the carrier with a uniform velocity. As gravity accelerates the drop, the inflow velocity is calculated using the following expression

$$U_{in}^{n+1} = U_{in}^{n} - \alpha V_{drop}^{n}\Big|_{frame} \tag{6}$$

with U_{in} the inflow velocity and V_{drop} the velocity of the drop in the moving reference frame. The constant α is a parameter used to specify how much the inflow velocity is corrected at each numerical iteration. With $\alpha = 0$, the inflow velocity is constant, and $\alpha = 1$ the full correction velocity is applied to the inflow velocity. Incorporating a strong correction parameter allows the simulation to respond quickly to a shift in the drop's location within the computational domain; however, the inflow velocity may change in response to non-physical, numerical velocity fluctuations and contribute to poor simulation results. Generally a value of $\alpha = 0.7$ was used.

The applicable boundary conditions are as follows. The diameter and location of the droplet were specified to define the initial location and shape of the gas-liquid interface. The computational domain was periodic in the x direction (and in z also if the model was 3D).

The Owkes and Desjardins' [3] VOF model, like other geometric VOF models, tracks the volume fraction of each fluid phase in each cell. It uses a flux-based, semi-Lagrangian transport scheme to update the liquid phase volume fraction between time steps. Flux volumes as shown in Figure 2 are defined as streak-tubes and can be transported back and forward in time along the streak-lines to determine the flux through each cell face between iterations. By defining a flux of volume fraction, the liquid volume fraction in a cell at the new time step is calculated.

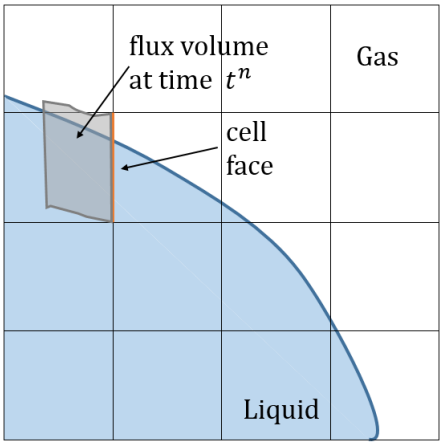

Figure 2: Portion of droplet within computational domain. The flux volume as transported backward in time passes through the indicated cell face between times steps t^n and t^{n+1}.

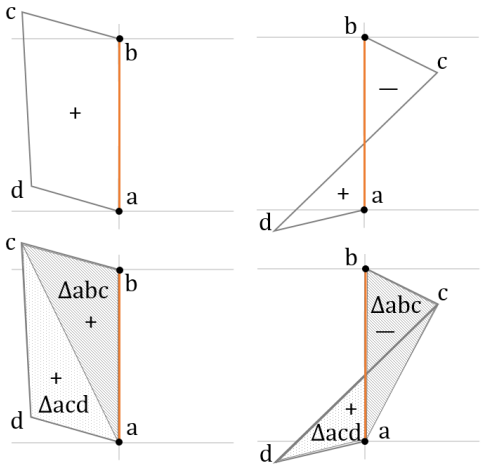

Figure 3: 2D example of Positive Flux and Mixed Flux simplex definitions. The line between points "a" and "b" represents the cell face.

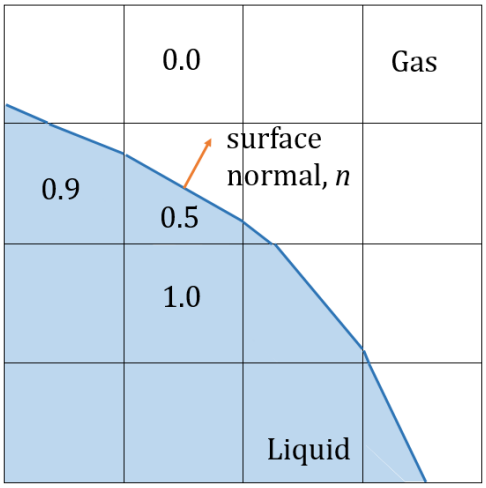

Figure 4: Interface reconstruction using the PLIC method: the percent volume fraction of liquid specifies the amount of fluid and the surface normal determines the orientation.

To compute the flux across a cell face, the flux volume is partitioned using geometrical operations into a collection of simplices (triangles or tetrahedra in 2D and 3D, respectively). One unique aspect of this approach is that it uses the corner vertices' velocity vectors for the transport method. As a result, the flux volumes are non-overlapping and conservation is ensured. Figure 3 shows two examples of the flux volume partitioning method in two-dimensions. Simplices are defined to determine both the sign and volume of flux crossing the face. The liquid volume fraction in a cell at the new time step is obtained by adding the fluxes for all faces of the cell. Most VOF methods struggle to compute this flux when a cell experiences both a positive and negative flux across a single face. As shown in the right side of Figure 3, the model used here needs only to divide the region into simplicies, determine the sign of the flux based on a convention (e.g., right hand rule), and compute the total flux to determine the liquid volume fraction in a cell at the next time step. Where the positive and negative simplex flux volumes overlap, they cancel each other and the true flux is obtained. This reduces the complicated geometry into a series of systematic geometric operations.

The PLIC method is then used to approximate the surface interface as a straight line or plane (in two or three-dimensions, respectively) whose normal determines the interface orientation. The reconstructed geometry is shown in Figure 4.

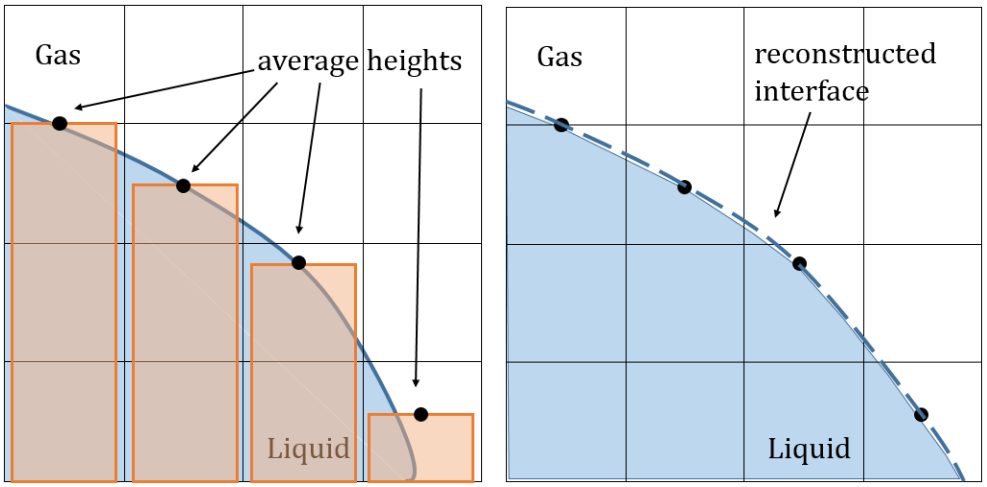

(a) Height columns that describe the surface interface.

(b) Reconstructed interface based on a parabolic curve fit through points.

Figure 5: Method of heights used to calculate curvature

The computation to obtain curvature, κ, used here is a modified version of the height function method [10]. Columns defining the average height of the amount of fluid in the direction most in line with the interface normal vector are used to define a set of points. The height values at these points are used with finite difference methods to calculate the curvature. Historically, this method is impractical for interfaces that deform significantly because the interface shape might not be oriented in any of the three directions, yielding a poor approximation. Popinet [14] introduced a scheme whereby heights and widths are combined to compute a parabolic curve-fit (Figure 5 shows the approximation for heights); this method yields improved results for interfaces with large curvatures. The modified version of the method of heights used here was developed by Owkes and Desjardins [15]. It orients the heights such that they are aligned with the surface normal. Though this is more computationally expensive, it provides an accurate curvature for under-resolved or highly curved interfaces.

4 Computational Results

The code developed by Prof. Desjardins' lab, NGA, was used to complete the simulations. It had been validated for the canonical Zalesak's disk model and is capable of modeling two phases with high density and viscosity ratios. Of note is that some of the simulations reported here are a 2D circle model. In three dimensions, this represents an infinitely long cylinder perpendicular to the flow stream, and not a falling sphere. As such, results from these cases cannot be directly compared to analytical and experimental droplet results.

The objective of this project was to focus on common liquids (density $\rho_l \sim 1000$ kg m^{-3} and viscosity $\mu_l \sim 10^{-3}$ N s m^{-2}) and gases ($\rho_g \sim 1$ kg m^{-3} and $\mu_g \sim \times 10^{-5}$ N s m^{-2}). At lower Reynolds numbers, drop deformation is less significant, making it easier to conduct code validation. Thus, the behavior was explored for $Re_D \sim 10$ and $We \sim 0.01$. The gas viscosity was increased to 10^{-4} N s m^{-2} to achieve the reduction in Reynolds number. Because Weber number is not a function of dynamic viscosity, this strategy effectively reduced the Reynolds

number of the flow, without making surface tension effects more dominant.

Figure 6 illustrates the inflow velocity behavior of a representative 1 mm drop. Even with a low Reynolds number, significant oscillations were observed (though steady flow was expected). In this case, the velocity fluctuations could be attributed partly to wake instability from deformation. However, for a 0.5 mm droplet test case, the droplet remained quite spherical, but the inflow velocity still oscillated significantly.

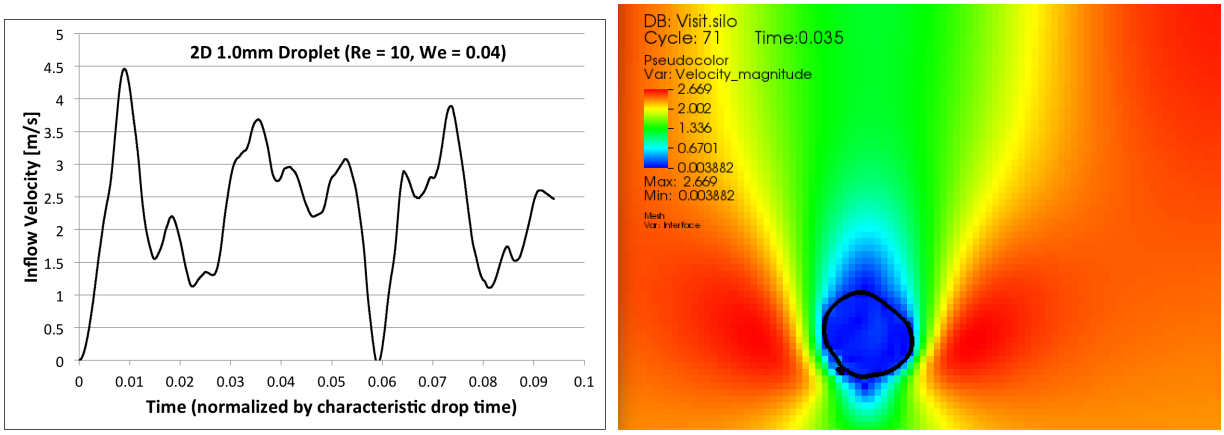

(a) Inflow velocity

(b) Velocity field showing deformation of interface.

Figure 6: Behavior of 1mm drop simulation with higher carrier phase viscosity. Note the continued presence of strong velocity oscillations.

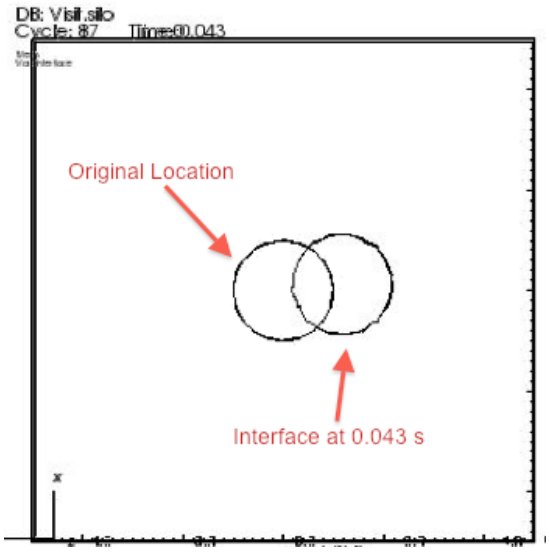

Figure 7: Movement of 0.5 mm drop with no gravity acting. Location of interface at start and end of simulation.

It was determined that the unsteady wake at low Reynolds number flows resulted from errors in curvature calculations. At this point, the modified method of heights as described earlier had not yet been implemented. Large density and viscosity ratios, combined with strong surface tension, yielded local accelerations on the drop surface when computing curvature. The expression used to calculate the inflow velocity viewed these local accelerations as overall changes in the drop's velocity within the moving reference frame and adjusted inflow accordingly.

To confirm that the curvature calculation was the driving cause of the unsteady behavior, the 0.5 mm case was computed without an applied gravity force. Without any external forces acting on the drop, one would expect the drop to remain stationary. However, as shown in Figure 7, it is clear that droplet moves over time. Additionally, refining the mesh and increasing the number of points used to calculate curvature did not improve the results: it took longer for these "computational vibrations" to occur, but when they did, they were much stronger. Further investigations showed that modifying the α parameter (i.e., $\alpha = 0.2, 0.7$, and 1) did not reduce the destabilizing accel-

erations. It was concluded that the computation of curvature required modification to obtain physically meaningful results.

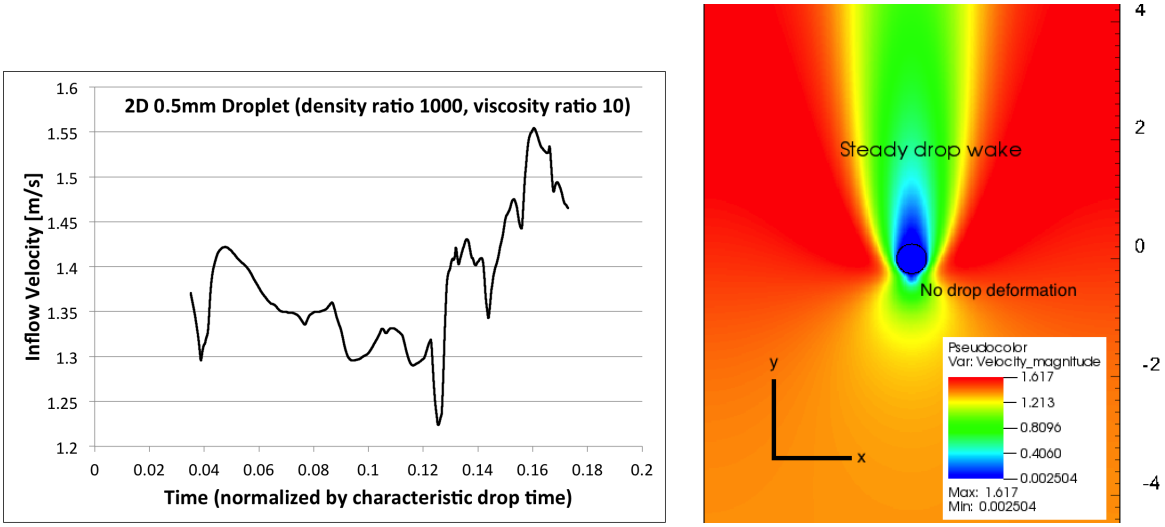

(a) Inflow velocity (b) Velocity field

Figure 8: Behavior of 2D 0.5 mm drop simulation with corrected curvature calculation.

The local accelerations may have also been partly attributable to the fact that these simulations were being run with a time-step such that the viscous Courant-Fridrichs-Lewy (CFL) >> 1. With the new curvature method implemented and a reduced time-step such that the viscous CFL $\sim$ 1, the drop displayed better stability as shown in Figure 8. The inflow velocity as given in Figure 8(a) is still fluctuating, but this is likely because the simulation was not completed up to the characteristic drop time; the flow is still in a transient period.

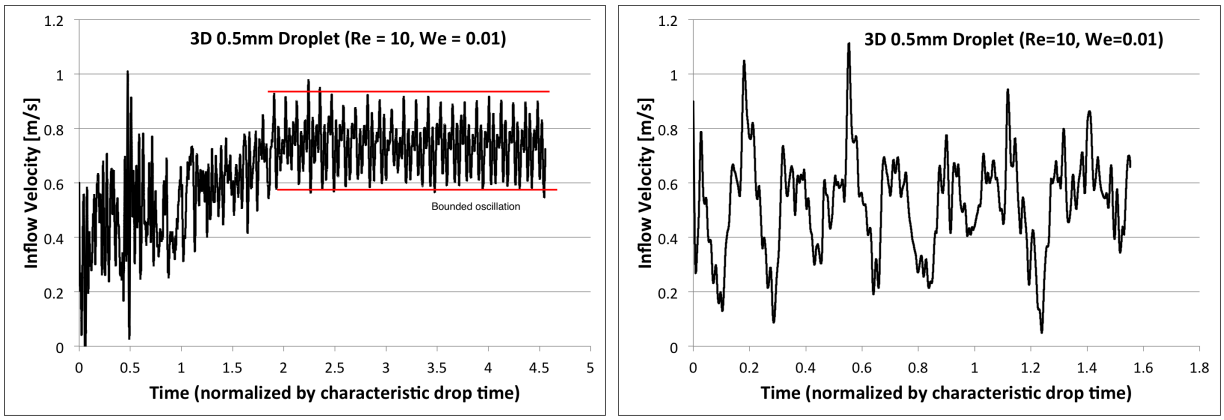

(a) Coarse mesh (8 cells/D) drop velocity (b) Refined mesh (15 cells/D) drop velocity

Figure 9: Inflow velocity of 3D droplet. $\rho = 1000$ and $\mu = 10$.

The 3D droplet models yielded improved results; the droplet experienced the "three-dimensional relieving effect" whereby the gas phase has a third dimension, and thus greater freedom, to pass by the drop. Using a model which resolved the droplet to approximately 8 computational cells across the droplet diameter, the inflow velocity oscillation was significantly reduced and the droplet remained relatively stationary. The velocity trend is given in Figure 9(a). The velocity oscillation was within approximately 10 % in excess and less than the average value at any given time once steady behavior was established. The average velocity after the transitory period had passed was approximately 0.8 m/s.

The mesh was further refined to 15 cells across the droplet diameter in effort to reduce the magnitude of the oscillations. The results shown in Figure 9(b) show the inflow velocity after approximately one and a half characteristic time lengths. It appears that the droplet had not reached expected behavior; however, further testing was not completed at this time.

5 Discussion

In the aforementioned computational experiments of a falling liquid drop, the numerical parameters of interest include classic variables such as mesh grid fineness and time step length, as well as case-specific parameters such as the damping coefficient α in the inflow velocity equation. As investigated in various simulations, it was determined that these parameters had some effect on the calculation results.

In this particular study, grid refinement received less attention because the focus was on attaining code functionality. Before investigating mesh dependency of solutions, it is important to confirm that predicted results are reasonable.

As reported in the Results section, the time step selection was an important factor in obtaining physically meaningful results. The CFL condition is used to make appropriate choices for the time step in simulations. The viscous CFL number, C, in one dimension is given as:

$$C = 4\mu \frac{\Delta t}{(\Delta x)^2} \tag{11}$$

where Δt is the time step, and Δx is the grid spacing. Specifically, it was observed that in the 2D simulations, the viscous CFL could not be greater than ~ 1 if local velocity fluctuations were to be avoided. The 3D cases did not require such a stringent requirement on this CFL number because of 3D relief behavior (viscous CFL was allowed to increase to ~ 30).

The parameter α, which specifies the percentage by which the inflow velocity changes to offset the velocity of the drop *within* the moving reference frame between each time step, did not impact the model significantly if $\alpha \approx 0.2$ or greater. As expected, the extremely small α values resulted in the droplet falling freely through the domain. For slightly larger values and above; however, the simulation was insensitive to variations in α. This was expected because the simulations focused on steady flow: with only small changes in velocity, the parameter α would not have a large impact. In unsteady simulations; however, α may have a greater impact on simulation results.

After observing the movement of the drop in the absence of any physical applied forces, it was determined that the numerical model struggled to compute curvature when surface tension was more dominant than inertial effects. Decreasing the surface tension forces (thereby increasing Weber number) relaxed the curvature calculations such that local velocity accelerations did not occur on the interface. As a result, the simulation achieved steady behavior. However, by increasing Weber number too significantly, the surface tension forces were too weak to maintain the drop's spherical shape, and it deformed and broke apart.

To verify the 3D results, the inflow velocity was compared to the terminal velocity prediction obtained from the differential governing equation for a heavy sphere subject to gravity

$$\frac{d\mathbf{u}}{dt} = \frac{f}{\tau_p}(\mathbf{u} - \mathbf{v}) + \mathbf{g} \tag{12}$$

where $\mathbf{u}$ is the background fluid velocity, $\mathbf{v}$ is the drop velocity, and τ_p is the characteristic particle response time

$$\tau_p = \frac{1}{18}\frac{\rho_d D^2}{\mu_c} \tag{13}$$

and f is the drag factor. In this case, for $Re = 10$, the Shiller-Nauman correlation was used

$$f_{SN} = 1 + 0.15Re^{0.687} \tag{14}$$

For a 0.5mm droplet with density of 1000 kg m^{-3}, viscosity of 10^{-3} N s m^{-2}, and surface tension of 0.0625 N m^{-1} falling through carrier phase with density 1 kg m^{-3} and viscosity 10^{-4} N s m^{-2}, the Shiller-Nauman correlation predicted a terminal velocity of 0.9 m/s.

The 3D model with a coarse mesh of 8 cells across the drop diameter yielded an average terminal velocity of 0.8 m/s with fluctuations plus/minus 10 percent of the average. Further testing would be necessary to determine if the refined mesh yielded results closer to the Shiller-Nauman prediction.

6 Conclusions

The behavior of falling drops has been widely studied in experimental work and in some simplifying analytical cases; however, numerical work has been relatively limited, particularly in the area of higher Reynolds numbers, when the droplet significantly deforms and even begins to break apart. This project focused on showing that the NGA code can track the behavior of liquid droplets falling in a quiescent gas where the two phases are characterized by large density and medium viscosity ratios: on the order of 1000 and 10, respectively.

The simulations conducted were of low Reynolds number (~ 10) and low Weber number ($\sim 0.01 - 1$) droplets. The 3D droplet model showed fairly good agreement with the Shiller-Nauman correlation for a falling liquid droplet. As a result of this project, a method for calculating the velocity of the moving reference frame traveling with the drop was developed, and the effect of different numerical parameters (e.g., the damping parameter α for the inflow velocity calculation) on the numerical model was investigated.

From this investigation, it is clear that there are several important requirements when modeling a falling liquid drop using this VOF scheme. First, a robust method of calculating and resolving the curvature of the drop in all the surface normal directions (particularly the normals oriented off of the Cartesian coordinate axes) should be employed. Appropriately sized time steps should be selected to maintain temporal accuracy of viscous dynamics. Finally, to capture three-dimensional relaxation effect and prevent the strong velocity fluctuations as observed in 2D, a 3D model with relatively good drop resolution is required.

The simulations discussed in this project are significantly limited in application: only steady flow (i.e., low Reynolds numbers) with a relatively low viscosity ratio and somewhat low Weber number were investigated. The density ratio of these flows is characteristic of common liquids and gases; however, the viscosity ratio is an order of magnitude smaller than what is common for liquids and gases. Future work in this area would be to complete a full regime mapping over a range of Reynolds and Weber numbers to characterize numerically the behavior of falling liquid drops, while verifying with the available experimental data.

Acknowledgements

The author wishes to thank Professor Olivier Desjardins and Mark Owkes for their invaluable support and guidance with this project.

References

[1] R.C. Clift, J. R. Grace, M.E. Weber, Bubbles Drops and Particles, Academic (1978).

[2] Beard K.V., Terminal Velocity and Shape of Cloud and Precipitation Drops Aloft, J. Atmos. Sci. 33 (1976) 851-864.

[3] Owkes M. and Desjardins O., A computational framework for conservative, three-dimensional, unsplit, geometric transport with application to the volume-of-fluid (VOF) method, J. of Comput. Phys. 270 (2014) 587-612.

[4] Gunn R. and Kinzer G.D., The Terminal Velocity of Fall for Water Droplets in Stagnant Air, J. Meteor. 6 (1949) 243-248.

[5] Beard K.V. and Pruppacher H.R., A Determination of the Terminal Velocity and Drag of Small Water Drops by Means of a Wind Tunnel, J. Atmos. Sci. 26 (1969) 1066-1072.

[6] McDonald J.E., The Shape and Aerodynamics of Large Raindrops, J. Meteor 11 (1954) 478-494.

[7] Taylor T.D. and Acrivos A., On the deformation and drag of a falling viscous drop at low Reynolds number, J. Fluid Mech. 18 (1964) 466-476

[8] Pruppacher H.R. and Pitter R.L., Semi-Empirical Determination of the Shape of Cloud and Rain Drops, J. Atmos. Sci. 28 (1971) 86-94.

[9] Feng J.Q., A deformable liquid drop falling through a quiescent gas at terminal velocity, J. Fluid Mech. 658 (2010) 438-462.

[10] DeBar R., Fundamentals of the KRAKEN code, Tech. Rep. UCIR-760, LLNL (1974).

[11] Nichols B. and Hirt C., Methods for calculating multi-dimensional, transient free surface flows past bodies, Tech. Rep. LA-UR-75-1932, Los Alamos National Laboratory (1975).

[12] Noh W.F. and Woodward P., SLIC (simple line interface calculation), in: Proceedings of the Fifth International Conference on Numerical Methods in Fluid Dynamics, no. 59 in Lect. Notes Phys., Springer Berlin Heidelberg, 1976, pp. 330-340.

[13] Osher S. and Sethian, J. A., Fronts propagating with curvature-dependent speed: Algorithms based on HamiltonJacobi formulations, J. Comput. Phys. 79 (1988) 1249.

[14] Popient S., An accurate adaptive solver for surface-tension-driven interfacial flows, J. Comput. Phys. 228 (16) (2009) 5838-5866.

[15] Owkes M. and Desjardins O., A mesh-decoupled height function method for computing interface curvature. Pre-print: submitted to J. of Comput. Phys. (2014).